34th Annual International Conference of the IEEE EMBS
San Diego, California USA, 28 August - 1 September, 2012

Automated Localization and Segmentation of Lung Tumor from PET-CT Thorax Volumes Based on Image Feature Analysis

Hui Cui, Xiuying Wang, Dagan Feng

Abstract—**Positron emission tomography - computed tomography (PET-CT) plays an essential role in early tumor detection, diagnosis, staging and treatment. Automated and more accurate lung tumor detection and delineation from PET-CT is challenging. In this paper, on the basis of quantitative analysis of contrast feature of PET volume in SUV (standardized uptake value), our method firstly automatically localized the lung tumor. Then based on analysing the surrounding CT features of the initial tumor definition, our decision strategy determines the tumor segmentation from CT or from PET. The algorithm has been validated on 20 PET-CT studies involving non-small cell lung cancer (NSCLC). Experimental results demonstrated that our method was able to segment the tumor when adjacent to mediastinum or chest wall, and the algorithm outperformed the other five lung segmentation methods in terms of overlapping measure.**

I. Introduction

LUNG cancer is one of the major causes of death from cancers [1]. Early diagnosis and staging of lung cancer is important to significantly increase the survival rate of lung cancer. Accurate lung tumor segmentation is of preliminary importance to lung cancer radiotherapy for avoiding damage to its neighbouring healthy organs or tissues. The hybrid PET-CT scanners, providing the complementary biological information at molecular level and anatomical structures from a same imaging session, have been widely utilized for lung cancer diagnosis and treatment.

In 18F-fluoro-deoxy-glucose (FDG) PET images, lung tumors can be distinguished as "hot spots" due to their high intensities representing the voxel activities. The standardized uptake value (SUV) provides a semi-quantitative measurement to normalize PET intensities across different acquisition times and varying patients. Therefore, PET is considered more effective than CT in terms of automated tumor detection. However, the automated localization of lung tumor based on SUV is challenging, mainly because normal organs such as liver and heart also exhibit an increased FDG uptake. Therefore, seed points or the bounding boxes are manually selected for the computerized lung tumor delineation from PET [2-4]. Another major obstacle to automated tumor delineation from PET is posed by the low spatial resolution and relatively low signal noise ratio (SNR) of PET.

Due to the better tumor boundary definition provided by anatomic CT, in clinical practices, manual delineation of tumor largely depends on CT image [5]. However, the low contrast between the soft tissues in CT raises a challenge for automatically separating the tumor from its neighbouring healthy tissues [6]. Based on image registration, better use of PET and CT information for tumor segmentation [7, 8]has been investigated. However, segmentation of the tumor when it extends or attaches to mediastinum or chest wall remains a challenge.

In our previous work [4], the tumor-customized downhill (TCD) method solved the tumor leakage into adjacent healthy tissues, and could delineate the whole tumor volume even when the tumor was heterogeneous. The SUV value and gradient were both considered for the stopping criterion. Several studies [6, 9-12] had investigated other features beyond gradient or SUV values in medical image analysis. For instance, in [6], Yu et al analyzed 14 PET and 15 CT textural features under the assumption that tumor and normal tissues may have different textures or patterns, and then developed a co-registered multimodality pattern analysis segmentation system in [9]. The texture features were used for merging after the watershed segmentation in [10].

In this paper, we presented an automated tumor localization and segmentation approach. Contrast feature was investigated and showed capability in the capture and localization of the tumor. Besides the decision strategy automatically classified the cases into two categories, and then the segmentation on PET or CT was accomplished correspondingly.

II. Method

A. Tumor Localization via Contrast Feature from PET volume in SUV

Because the neighbourhood grey-tone difference matrix (NGTDM) [13] takes spatial relationship and probabilities of intensities into consideration, it reveals more information than first order features like mean, standard deviation and gradient. Among all the features based on NGTDM, contrast is a reflection of the intensity difference between neighbouring regions. In addition, the spatial frequency of the changes in intensity can be reflected by contrast. Therefore, in our method, the contrast feature is calculated from PET SUV volume.

The calculation of contrast [13] in PET volume is on a voxel-by-voxel basis. Three-dimensional (3D) windows surrounding each voxel in turn are defined. In our

H. Cui is with the Biomedical and Multimedia Information Technology (BMIT) research group, School of Information Technologies, The University of Sydney, Australia (e-mail: hcui7511@uni.sydney.edu.au).

X. Wang is with the BMIT research group, The University of Sydney, Australia (e-mail: xiuying@it.usyd.edu.au).

D. Feng is with the BMIT research group, Australia and with the Center for Multimedia Signal Processing (CMSP), Department of Electronic & Information Engineering, Hong Kong Polytechnic University, Hong Kong, and also with the Med-X Research Institute, Shanghai Jiao Tong University (e-mail: feng@it.usyd.edu.au).

experiments, the contrast for a voxel $v_{(x,y,z)}$ is calculated within the 3D window $R_{x,y,z}$ with size of $l \times w \times h$. $\forall i, \Phi_i = \{v_{k,r,s} \mid v(k,r,s) = i \,\&\, v_{k,r,s} \in R_{x,y,z}\}$.

Then i th entry in the NGTDM is

$$S(i) = \begin{cases} \sum |I - \bar{A}_i|, & \Phi_i \neq 0 \\ 0, & otherwise \end{cases} \quad (1)$$

where A_l is the average grey-tone of the neighbourhood of $v_{(k,r,s)}$, $R_{k,r,s} \subseteq R_{x,y,z}$

$$\bar{A}_i = \bar{A}(k,r,s) = \frac{1}{\omega - 1} \times \left[\sum_{m=-\alpha}^{\alpha} \sum_{n=-\beta}^{\beta} \sum_{p=-\gamma}^{\gamma} f(k+m, r+n, s+p) \right] \quad (2)$$

$$\omega = (\alpha+1) \times (\beta+1) \times (\gamma+1) - q \quad (3)$$

$$q = count\{(k+m, r+n, s+p) \notin R_{k,r,s}\} \quad (4)$$

Then the contrast is defined as

$$Contrast = \left[\frac{1}{N_g (N_g - 1)} \sum_{I=0}^{G_h} \sum_{J=0}^{G_h} p_I p_J (I-J)^2 \right] \times \left[\frac{1}{N^2} \sum_{I=0}^{G_h} S(i) \right] \quad (5)$$

where $N_g = \sum_{i=0}^{G_h} Q_i, p_i = \frac{N_i}{N^2}, Q = \begin{cases} 1, p_i \neq 0 \\ 0, otherwise \end{cases}$

$$N = (l+1) \times (w+1) \times (h+1) - \Omega \quad (6)$$

$$\Omega = count\{(x+l, y+w, z+h) \notin R_{x,y,z}\} \quad (7)$$

As shown in Fig. 1, there are multiple hotspots in PET volume in SUV, and the tumor cannot be directly localized solely based on detecting the highest SUV. After calculating the contrast feature (Fig.1 (c)) from PET, only the tumor region presents the highest contrast value, while the mediastinum could be filtered out. It is because the contrast takes into account the information of the neighbouring voxels and the more similar values the neighbouring voxels exhibit, the lower contrast. Therefore, PET contrast has the capability of reflecting the location of tumor in thorax volume, and the tumor can be automatically localized by identifying the highest contrast value.

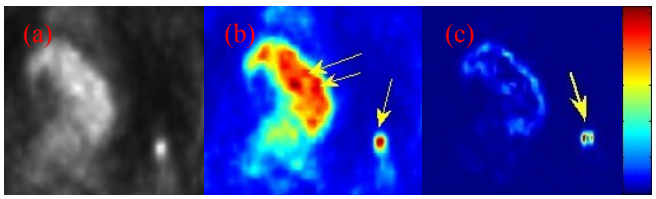

Figure 1.Analysis of PET volume in SUV and PET contrast. (a) PET volume in SUV. (b) PET volume represented in pseudo colours (c) the corresponding PET volume in contrast. Color bar shows that the red colour corresponds to the maximum value and the blue for the minimum.

After the tumor being localized, its boundary definition in PET images is implemented based on our previous work (TCD) [4], because it is capable of segmenting and separating tumors even when they are adjacent to other tissues.

B. Decision and Classification Strategy for Tumor Segmentation from PET or CT

In order to make full use of the advantages of PET and CT images according to different cases respectively, our algorithm includes a decision scheme for automatic classification of the studies into simple cases or complicated cases. The simple cases indicate that the tumor is clearly separate or "isolated" from other tissues/organs, and therefore its boundary can be clearly identified on CT. Hence, the segmentation can be based on CT. The complicated case means that the tumor may be adjacent to mediastinum or attached to chest wall, and CT is less helpful for boundary definition, and therefore, the segmentation would depend on PET.

Boundary expansion on PET: In order to automatically classify the studies, we expand the tumor boundary by TCD to include more surrounding tissues or structures. This boundary expansion is obtained by including voxels with 20% maximum SUV value (maxSUV) to compensate TCD delineation in which voxels with or less than 20% maxSUV are excluded as non-tumor tissues.

Decision strategy based on CT: The boundary expansion is mapped onto CT and the decision making region (DMR) is defined as the region between the initial boundary and the expansion boundary. Because intensity distributions of lung region are substantially different from those of chest wall or the mediastinum, and the difference of the intensity distributions between DMR and the lung can be used as reference for decision making. If the distribution of DMR is similar to lung region, then the tumor is considered as isolated or a simple case (Fig. 2 (a)). Otherwise, it is a complicated case (Fig. 2 (b), (c)). Accordingly, the segmentation makes full usage of CT or depends on PET.

C. Algorithm

```
Algorithm: Lung Tumor Localization and Segmentation
Input: PET SUV volume and CT volume
Output: Tumor delineation on PET-CT volumes
1 Tumor localization and definition
  (1) Calculate contrast in PET volume
  (2) Tumor localization by the highest contrast
  (3) Tumor definition by TCD
2 Decision strategy for tumor segmentation from PET
  or CT
  (1) Expand tumor region with a threshold of 20% of
      maximum SUV;
  (2) Map the PET tumor expansion region onto CT
      volume to define DMR
  (3) If (DMR and lung have similar distributions){
        The tumor is isolated from the surroundings
        Tumor segmentation from CT
      }
      Else {
        The tumor is in close proximity of
        surrounding structures such as mediastinum
        or chest wall.
        Tumor segmentation from PET
      }
```

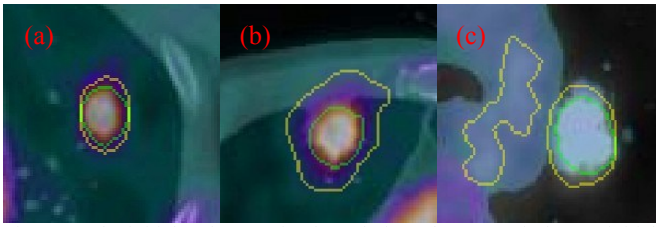

Figure 2. The initial and expansion boundaries. The green circles are initial boundaries. The yellow circles are expansion boundaries. Tumor (a) is isolated and marked as simple case. (b) and (c) complicated cases. (b) attached to chest wall, (c) adjacent to mediastinum.

III. Experiments and Discussion

A. Clinical Data

We used 20 thorax PET-CT NSCLC studies from a Biographic True V 64-slice PET-CT scanner (Siemens Medical Solutions). The CT scans were reconstructed using a matrix of 512 × 512 pixels with pixel size of 0.98 mm × 0.98 mm × 2 mm. The PET scans were reconstructed using a matrix of 168 × 168 pixels with pixel size of 4.07 mm × 4.07 mm × 2 mm. Among the 20 datasets, there are 14 simple cases, six complicated cases, including four chest wall cases, and two mediastinum cases. The PET is rescaled to the same size of its corresponding CT during their mapping stage.

B. Contrast Feature Analysis

In order to investigate the contrast features of tumor and other tissues, 10 datasets with manually delineated tumor contours by clinics were used. The contrast values were divided into two groups, the tumor and other parts of the thorax, including the mediastinum and chest wall. Fig. 3 is the histogram distribution analysis of the contrast features and demonstrates that the tumors always present high contrast values.

C. Quantitative Validation

We compared our approach with five other delineation methods: 1) a threshold of 40% of maximum SUV, referred as RG40; 2) a threshold of 50% of maximum SUV, referred as RG50; 3) Fuzzy C-means with two clusters, referred as FCM; 4) the watershed, referred as WS; 5) TCD; and our method was referred as DM. The overlap between each case and its corresponding ground truth was calculated using Dice's similarity coefficient (DSC) as (8):

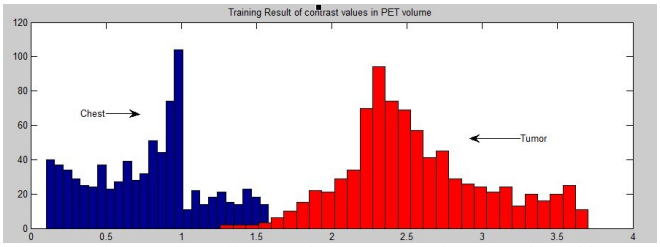

Figure 3. Histogram Distribution of PET contrast features. The red bars are tumor samples, and the blue bars represent the other thorax tissues. 795 tumor samples and randomly selected 900 other thorax tissues samples. The horizontal axis represents the value of contrast feature, and the vertical axis the quantity of samples.

$$DSC(V_1, V_2) = \frac{2|V_1 \cap V_2|}{|V_1| + |V_2|} \tag{8}$$

where V1 was the ground truth, V2 was the volume obtained from each of the delineation approach.

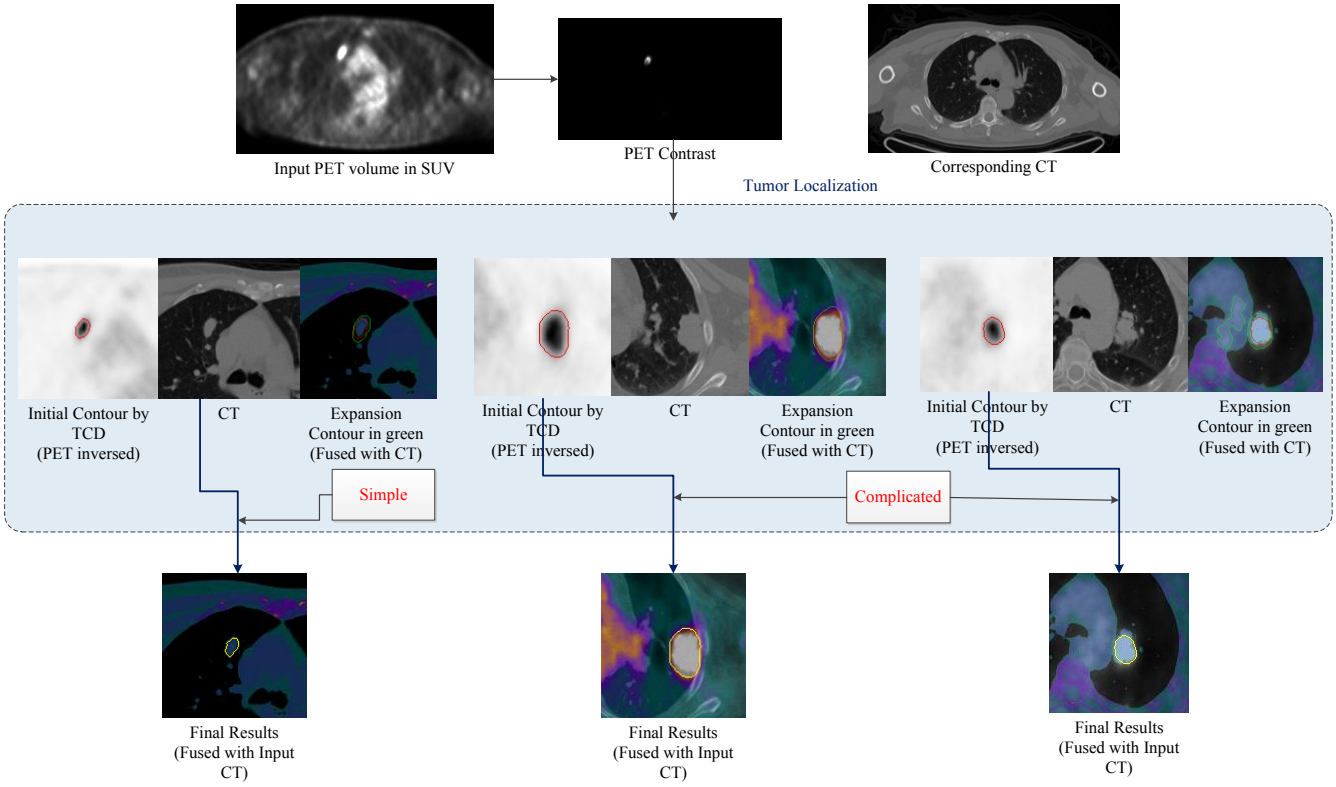

Figure 4. Automated localization and segmentation of lung tumor

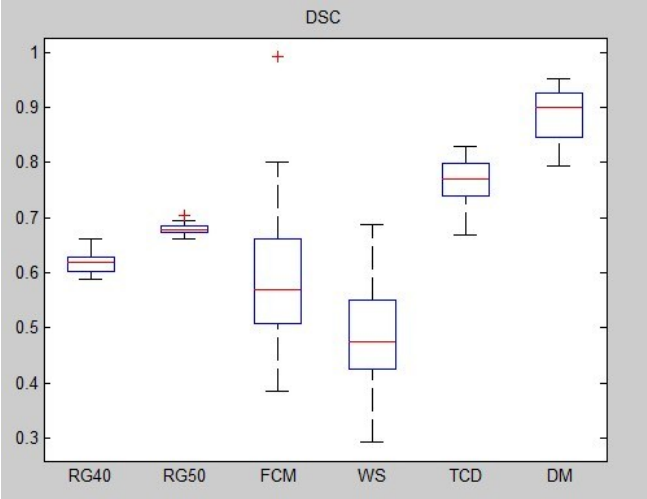

Figure 5. Dice's similarity coefficient (DSC) of six different approaches over 20 datasets.

Fig. 4 illustrates the tumor segmentation procedure by our algorithm.

The DSC comparison of the six approaches was shown in Fig. 5. DM achieved the highest average DSC of 0.89, followed by TCD of 0.78. The reason for the increased segmentation accuracy is that in DM, for the simple cases (with DSC of 0.94), the segmentation was performed on CT images that provide better boundary definition.

IV. Conclusion

Our automated tumor localization and segmentation method utilized PET and CT images features including PET SUV, gradients, contrast and CT intensity distribution. The PET contrast was valuable in automatic tumor localization; SUV and gradients served for tumor delineation from PET; and CT intensity distribution was effective in decision and classification of tumor cases. This automatic approach made a better use of complementary PET-CT information to achieve improved tumor segmentation. Experimental results validated that our algorithm outperformed its counterpart methods in terms of DSC measure.

Acknowledgment

This research is supported by ARC and PolyU grants.

References

[1] F. B. Ahmedin Jemal, Melissa M. Center, Jacques Ferlay, Elizabeth Ward and David Forman, "Global cancer satatistics," *CA: A Cancer Journal for Clinicians,* vol. 61, pp. 69-90, 2011.

[2] M. Hatt, C. C. L. Rest, N. Albarghach, O. Pradier, and D. VIsvikis, "PET functional volume delineation: a robustness and repeatability study," *European Journal of Nuclear Medicine and Molecular Imaging,* vol. 38, pp. 633-72, 2011.

[3] E. Day, J. Betler, D. Parda, B. Reitz, A. Kirichenko, S. Mohammadi, and M. Miften, "A region growing method for tumor volume segmentation on PET images for rectal and anal cancer patients," *Medical Physics,* vol. 36, pp. 4349-4358, Oct 2009.

[4] C. Ballangan, X. Wang, M. Fulham, S. Eberl, Y. Yin, and D. Feng, "Automated Delineation of Lung Tumors in PET Images Based on Monotonicity and a Tumor-Customized Criterion," *IEEE Transactions on Information Technology in Biomedicine,* vol. 15, pp. 691-702, Sept. 2011.

[5] J. S. Cooper, S. K. Mukherji, A. Y. Toledano, C. Beldon, I. M. Schmalfuss, R. Amdur, S. Sailer, L. A. Loevner, P. Kousouboris, K. K. Ang, J. Cormack, and J. Sicks, "An evaluation of the variability of tumor-shape definition derived by experienced observers from CT images of supraglottic carcinomas (ACRIN protocol 6658)," *International Journal of Radiation Oncology Biology Physics,* vol. 67, pp. 972-975, Mar 15 2007.

[6] H. Yu, C. Caldwell, K. Mah, and D. Mozeg, "Coregistered FDG PET/CT-Based Textural Characterization of Head and Neck Cancer for Radiation Treatment Planning," *IEEE Transactions on Medical Imaging,* vol. 28, pp. 374-383, March 2009.

[7] D. Han, J. Bayouth, Q. Song, A. Taurani, M. Sonka, J. Buatti, and X. Wu, "Globally optimal tumor segmentation in PET-CT images: a graph-based co-segmentation method," *Information processing in medical imaging,* vol. 22, pp. 245-56, 2011.

[8] V. Potesil, X. Huang, and X. S. Zhou, "Automated tumour delineation using joint PET/CT information," in *Medical Imaging 2007: Computer-Aided Diagnosis, Pts 1 and 2*. vol. 6514, M. L. K. N. Giger, Ed., ed, 2007, pp. Y5142-Y5142.

[9] H. Yu, C. Caldwell, K. Mah, I. Poon, J. Balogh, R. MacKenzie, N. Khaouam, and R. Tirona, "Automated radiation targeting in head-and-neck cancer using region-based texture analysis of PET and CT images," *International Journal of Radiation Oncology Biology Physics,* vol. 75, pp. 618-625, 2009.

[10] H. P. Ng, S. Huang, S. H. Ong, K. W. C. Foong, P. S. Goh, and W. L. Nowinski, "Medical Image Segmentation Using Watershed Segmentation with Texture-Based Region Merging," presented at the 2008 30th Annual International Conference of the Ieee Engineering in Medicine and Biology Society, Vols 1-8, New York, 2008.

[11] B. Ganeshan, S. Abaleke, R. C. D. Young, C. R. Chatwin, and K. A. Miles, "Texture analysis of non-small cell lung cancer on unenhanced computed tomography: initial evidence for a relationship with tumour glucose metabolism and stage," *cancer imaging,* vol. 10, pp. 137-143, 2010.

[12] J. Zhang, W. Zhang, C. Chen, Y. Guan, and C. Wang, "Computed Diagnosis System for Lung Tumor Detection based on PET/CT Images," presented at the 2010 3rd International Conference on Biomedical Engineering and Informatics (BMEI 2010) 2010.

[13] M. Amadasun and R. King, "Textural features corresponding to textural properties," *Systems, Man and Cybernetics, IEEE Transactions on,* vol. 19, pp. 1264-1274, 1989.